

Influence of annealing temperature on performance of dye-sensitized TiO₂ nanorod solar cells

X. Q. Gu · Y. L. Zhao · Y. H. Qiang

Received: 23 October 2011 / Accepted: 12 December 2011 / Published online: 21 December 2011
© Springer Science+Business Media, LLC 2011

Abstract Single-crystal rutile TiO₂ nanorod (NR) arrays have been synthesized on the fluorine-doped tin oxide substrates, followed by an annealing at 200–600 °C. It is found that DSSCs fabricated using TiO₂ NR arrays which undergo annealing display an increased efficiency than those that do not undergo annealing. The optimal efficiency of 4.42% power conversion is achieved in the DSSC made with 500 °C annealed arrays, which show a 450% increase in the overall conversion efficiency. The improvement is ascribed to the increased light harvesting, the enhanced electric contact and the suppressed recombination of the injected electrons with redox species in the electrolyte.

1 Introduction

Dye sensitized solar cells (DSSC) have received a worldwide attention as they offer the possibility of extremely inexpensive and efficient solar energy conversion [1–3]. Currently, limited by a low photo-to-electricity conversion efficiency and long-term stability, there is still a long way for the commercialization of this type of solar cells. Although their efficiencies have been reported to reach 12.3% in a very recent report [4], the value is still much lower than the p-n junction based counterparts. In general,

a typical DSSC device consists of a TiO₂ photoanode sensitized by a monolayer of dye molecules. Much effort has been devoted to optimize the morphology and structure of the photoanode for achieving a better cell performance (both in efficiency and stability). Traditionally, the anode is composed of randomly packed TiO₂ nanoparticles (NPs) with particle sizes of 10–20 nm [5–7], which have an advantage of high surface to volume ratios. Nevertheless, the slow electron transport as well as the poor adhesion to substrate greatly limits the cell performance [8–10]. For instance, the NP film thickness is always no more than 20 μm. Increasing the thickness would lead to a decrease of the overall photoelectric conversion efficiency due to a larger loss from electron recombination, since the electron diffusion length is limited.

Highly oriented 1D TiO₂ nanostructures grown on transparent conductive substrates may present a solution to these challenges [11, 12]. The structure represents an ideal channel for electrical carrier transport and is suitable for device integration. The electrons are transferred and collected through a direct channel rather than a disordered network structure constructed by NPs. In fact, Jennings et al. [13] have estimated the electron diffusion length was over 100 μm in TiO₂ nanotube (NT) cells, which are at least five times higher than that in the NPs based cells [14]. The diffusion length of electrons is expected to be much longer in the ordered TiO₂ single-crystalline NRs owing to a defect-free structure. There have been a few reports on DSSCs made with TiO₂ NR or nanowire (NW) arrays [11, 15–20]. Feng and his co-workers synthesized the densely packed single crystal TiO₂ NW arrays on FTO glass by hydrolysis of Ti precursors [15]. In their report, a high efficiency of ~5.02% was achieved in the DSSCs fabricated using only 2–3 μm long NWs. Besides, Liu et al. [11] also reported on the preparation of single crystal TiO₂ NR

X. Q. Gu (✉) · Y. L. Zhao · Y. H. Qiang (✉)
School of Materials Science and Engineering, China University of Mining and Technology, Xuzhou 221116, China
e-mail: xqgu@cumt.edu.cn

Y. H. Qiang
e-mail: yhqiang@cumt.edu.cn

X. Q. Gu
State Key Laboratory of Silicon, Zhejiang University, Hangzhou 310027, China

array on FTO coated glass and achieving a solar cell efficiency of 3.0% when using a 4 μm thick NR array as the photoanode. In another paper from their group, the oriented single crystalline TiO_2 NWs were prepared on a Ti foil and a power conversion efficiency of $\sim 1.4\%$ was achieved [16]. In these cases, TiO_2 NR arrays were grown directly on the conductive substrates in a one-step, low temperature solution process, which not only reduce the manufacturing cost, but also enhance the adhesion between TiO_2 and FTO layers. In spite of these advantages, the efficiency of the NR cells remains much lower than that of the NP cells. One important reason is that TiO_2 has an isotropous crystal structure and symmetry, which makes it very difficult to achieve a longitudinal structure. Several attempts has been made to improve their surface area, such as immersing the samples in NbCl_5 or TiCl_4 solution followed by a post-heating treatment at 500 $^\circ\text{C}$, leading to the corresponding improvement of 25% [15] and 50% [11] in the cell efficiencies, respectively.

In this work, highly ordered and aligned TiO_2 single-crystalline NR arrays were prepared on the FTO substrates, followed by annealing at 200–600 $^\circ\text{C}$. Afterwards, both the as-prepared and annealed samples were used as the photoanodes for the assembly of the DSSCs. It was found that the cell performance was strongly dependent on the annealing temperature (T_a). The highest conversion efficiency of 4.41% was achieved when the NR arrays were annealed in air at 500 $^\circ\text{C}$. By contrast, the un-sintered cells exhibited a low efficiency of 0.98% power conversion.

2 Experiment

2.1 Fabrication of TiO_2 NR arrays

Single crystal TiO_2 NR arrays are synthesized on FTO glass by a simple one-step hydrothermal method [11]. Briefly, the clean FTO substrates are placed in a sealed autoclave (60 mL volume), containing 0.6 mL of tetrabutyl titanate, 15 mL of hydrochloric acid (37 wt%) and 15 mL of DI water. The substrates were placed horizontal relative to the base of the autoclave, with the conducting side facing up. The synthesis is carried out at 150 $^\circ\text{C}$ and for 11 h, followed by the calcination in air at 200–600 $^\circ\text{C}$ for 30 min.

2.2 Device assembly

The resulting TiO_2 samples are immersed in a 0.3 mmol ethanolic solution of N719 at 80 $^\circ\text{C}$ for 2 h to complete the dye adsorption. Next, a DSSC device is assembled by sandwiching together a TiO_2 electrode and a 20 nm thick Pt-coated FTO. The electrodes are separated by a 60 μm

thick thermal-plastic Suryln spacer. A commercially available ionic electrolyte solution (Dalian Hepta Chroma) is infiltrated into the space between the electrodes by capillary action using a fine 1 mL syringe. The electrolyte contains 0.6 M 1-butyl-3-methylimidazolium iodide, 0.03 M I_2 , 0.5 M tert-butylpyridine, and 0.1 M guanidinium thiocyanate in acetonitrile/valeronitrile 85/15 (volume).

2.3 Characterization

The crystal structure and morphologies of the TiO_2 nanorods are examined by X-ray diffraction (XRD, D8), field emission scanning electron microscopy (FESEM, Sirion 200), high resolution transmission electron microscopy (HRTEM, JEOL-2010). The current density–voltage (J – V) measurements are carried out in dark and under illumination of 60 mW cm^{-2} , respectively using a Keithley model 2420 digital source meter. The simulated sunlight is provided by a 500 W Xe lamp fitted with an AM-1.5 filter (Beijing Trusttech). The active area of the DSSCs is fixed to 0.20 cm^2 by a light shading mask.

3 Results and discussion

3.1 Crystal structure and morphology

Figure 1a, b are the top-surface and cross-sectional FESEM images of the as-synthesized TiO_2 NR arrays, respectively. Both the images show a highly uniform, vertically aligned and densely packed array of NRs with flat tetragonal crystallographic planes. The NR array is grown on the FTO layer directly with an average length of $\sim 1.8 \mu\text{m}$. Figure 1c is a HRTEM image of a TiO_2 NR selected randomly. The measured inter-planar distance of 0.33 nm correspond to the TiO_2 (110) planes, suggesting that the single-crystal NR grows preferentially along the [002] direction. It is also observed that the NR surface is very clean and abrupt. Figure 1d shows the XRD pattern of TiO_2 NR array. As seen, the NRs have a crystal structure of single rutile phase with the enhanced (101) and (002) peaks, which is consistent with the results obtained from the SEM and TEM characterizations.

3.2 Photovoltaic performance

Figure 2 shows the J – V curves under illumination of DSSCs containing the as-prepared and sintered TiO_2 NR arrays. The open circuit voltage (V_{OC}), short circuit current density (J_{SC}), fill factor (FF) and conversion efficiency (η) are summarized in Table 1. These data were collected from one kind of samples prepared in the same route (including the growth condition and assembly process) so that the

Fig. 1 Top view (a), cross-sectional view (b) of FESEM images, HRTEM image (c), and XRD pattern (d) of TiO₂ NRs grown at 150 °C for 11 h by hydrothermal method

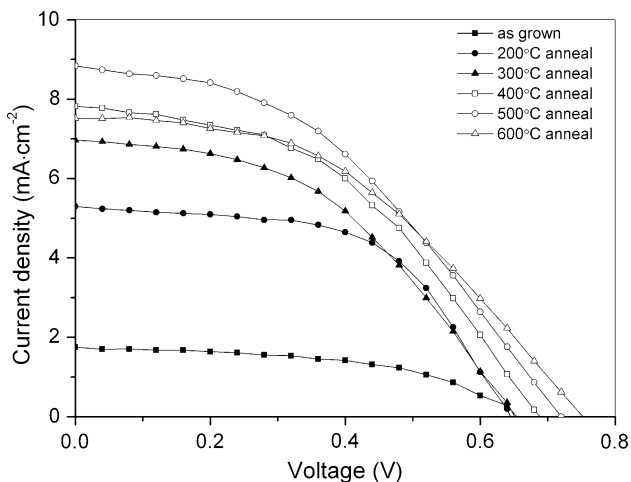
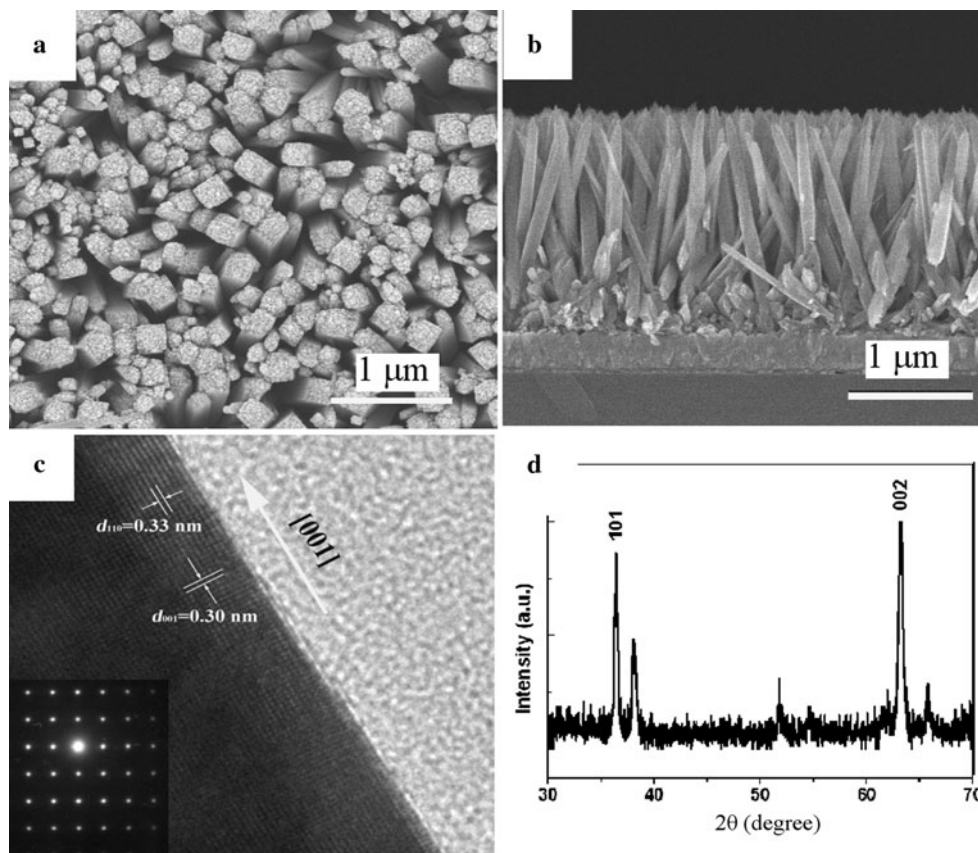


Fig. 2 *J*–*V* curves under illumination of DSSCs made with TiO₂ NRs annealed at RT–600 °C

experimental error caused by the operation or other accidental factors was as small as possible. As seen, the DSSC made with as-prepared TiO₂ arrays shows a η of $\sim 0.98\%$. By annealing the sample at 200 °C, η is increased to 3.22%, which is mainly ascribed to a large increase in J_{SC} . Increasing the annealing temperature (T_a) from 200 to 500 °C, both the increase of J_{SC} and V_{OC} is observed from

Table 1 J_{SC} , V_{OC} , FF and η of TiO₂ NR DSSCs as a function of T_a under an AM 1.5 illumination (60 mW cm⁻²)

T (°C)	J_{SC} (mA cm ⁻²)	V_{OC} (V)	FF	η (%)
RT	1.75	0.65	0.52	0.98
200	5.30	0.65	0.56	3.22
300	6.97	0.65	0.49	3.68
400	7.82	0.70	0.44	4.00
500	8.84	0.73	0.41	4.42
600	7.52	0.77	0.44	4.17

5.30 mA cm⁻² and 0.65 V to 8.84 mA cm⁻² and 0.70 V respectively, while FF is found to reduce from 0.56 to 0.41. As a result, the cell efficiency of 4.42% obtained at 500 °C demonstrates a 450% enhancement over the cells fabricated with as-grown samples. With further increasing T_a to 600 °C, J_{SC} decreases to 7.52 mA cm⁻² while V_{OC} increases to 0.77 V, leading to a little smaller conversion efficiency of $\eta = 4.17\%$.

3.3 Mechanism underlying the change of J_{SC} , V_{OC} , FF and η

As well known, the performance of TiO₂ NR DSSCs is mainly determined by the light harvesting, electron

transport and collection. The detailed mechanism is revealed as following:

3.3.1 Light harvesting

Light harvesting is an important factor that influences the light-to-electricity efficiency of DSSCs [21]. It is known that the light harvesting is strongly dependent on the efficient surface area for anchoring dye molecules. In this work, the annealing process has been demonstrated as an efficient way to improve the performance of DSSCs. It is because that a number of water molecules are absorbed on the surface of the as-grown TiO₂ NR arrays. The water molecules are removed by annealing, leading to the increased surface sites for anchoring dye. As a result, higher values of J_{SC} and V_{OC} are expected after annealing. Such a behavior has been demonstrated by a comparison of UV–visible absorption spectra indicated in our previous report [22]. In that report, the dye-sensitized TiO₂ NR array which underwent annealing exhibited a higher absorption coefficient over the visible band than that which didn't undergo annealing. Besides, the increase of dye absorption facilitates suppressing the charge recombination at the TiO₂/electrolyte interfaces, which contributes to the increase of J_{SC} and V_{OC} .

3.3.2 Electron injection/recombination on the dye/TiO₂ interface

Generally, the electron injection from the excited dye to TiO₂ can be finished in about 50 fs. Thus, the injection efficiency is strongly dependent on the recombination rate of the charges at the TiO₂/dye/electrolyte interface. In other words, a slower recombination means a more efficient injection of the electrons. Figure 3 compares the

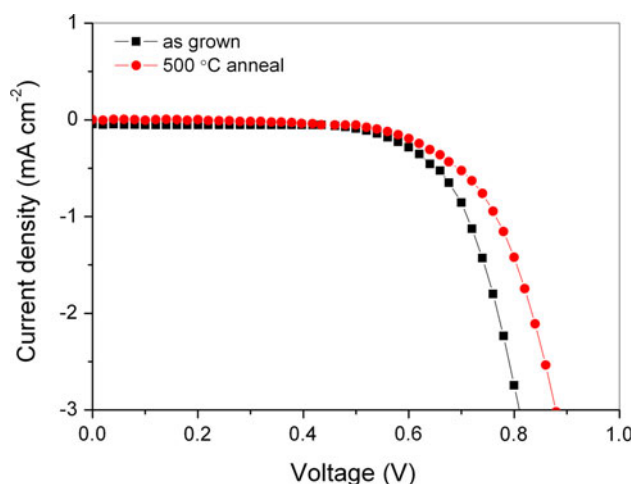


Fig. 3 J - V curves in dark of DSSCs made with the as-grown and 500 °C annealed TiO₂ NRs

voltage-dependent dark current curves of DSSCs made with the as-grown and the sintered samples. The dark current mainly results from the back transfer process occurring at the interface, which typically represents the recombination between the electrons in the conduction band and the I₃⁻ in the electrolyte [23–25]. As indicated in these curves, the sample which underwent annealing show a lower dark current and a higher onset voltage than the as-grown one, when these samples were assembled into the DSSCs. It suggests that the charge recombination was suppressed a lot after annealing. As a result, a more efficient electron injection is obtained, leading to the increase of J_{SC} , V_{OC} and η [26].

3.3.3 Electron transport/collection

It is clear that TiO₂ anode plays two roles in a DSSC: harvest the sunlight and carry the injected electrons. Thus, the transport rate of electrons is another important characteristic of TiO₂ photoanodes. Although the obtained NRs show a single crystal structure, a few defaults or defects may be produced in the surface/interface regions during the growth process. For instance, the injected electrons may be trapped by these defects presented on the surface and interface of NRs, resulting in a lowering of the transport rate. In addition, the transporting electrons may be blocked easily at the TiO₂/FTO interface due to a poor adhesion or electric contact. As a result, the annealing process not only facilitates reducing the number of oxygen vacancies, but also improves the interface adhesion, leading to the increase in J_{SC} and η .

3.3.4 Variation in FF with T_a

In our DSSC, the major factor that limits the efficiency is the low FF. FF is 0.52 for the un-sintered NR cell, which is much lower than the NP cells (always 0.75–0.85) [1]. It is known that FF which is defined as $J_{max} \cdot V_{max}/J_{SC} \cdot V_{OC}$ is attenuated by the total sheet resistance of a solar cell, including the series resistance (R_s) and the shunt resistance (R_{sh}). The values of R_s and R_{sh} are related to the poor surface/interface quality which may be introduced during the assembly process of DSSCs. Specifically, a low FF suggests that there may be either a high R_s or a low R_{sh} in the DSSC. With increasing T_a to 500 °C, FF decreases to 0.41 (see Table 1). Herein, the lowering of FF for the sintered cells with respect to the un-sintered ones is mainly attributed to the increase of both J_{SC} and V_{OC} , which can be explained by the terms of Ohm's law and the equivalent circuit model of a DSSC [27]. In details, after annealing, the increase in J_{SC} will result in an increased voltage drop across R_s and a decreased maximum voltage (V_{max}) output the external circuit. The behavior has been observed in the

DSSCs under the various illumination intensities as well by Grätzel's group [28]. In their reports, it was found that FF got reduced gradually with improving the illumination intensity.

Based on the aforementioned discussion, it is reasonable to speculate that the increase of J_{SC} with elevating T_a to 500 °C results from the improved light trapping, the enhanced electron injection and transport, as well as the suppressed electron recombination. With further elevating T_a to 600 °C, a slight lowering of J_{SC} is possibly ascribed to the increased sheet resistance of FTO. As is well known, V_{OC} is related mainly to the electron concentration in the conduction band of TiO_2 [29]. Hence, the increase of V_{OC} over the range of RT–600°C can be mainly ascribed to the increased electron injection or the reduced recombination of electrons [22].

4 Conclusion

The influence of T_a (200–600 °C) has been investigated on the performance of TiO_2 NR related DSSCs. The highest efficiency of 4.42% power conversion has been obtained in the solar cell made with 500 °C annealed TiO_2 NR arrays, which is 450% higher than that made with as-grown NR arrays. Such a large improvement is attributed to a higher amount of dye absorption, a faster electron transport and a lower charge recombination after annealing. We hope our work will shed light on understanding the transport mechanism of the electrons in TiO_2 electrodes.

Acknowledgments This work was financially supported by Youth Foundation of China University of Mining and Technology ON 091273, Climbing Program of China University of Mining and Technology ON 090237. The authors also thank Mr. Shengquan Fu and Mr. Shuyuan Zhang from China University of Science and Technology for assistance to the FESEM and HRTEM characterization and analysis.

References

1. B. O'Regan, M. Grätzel, *Nature* **353**, 737 (1991)
2. M.K. Nazeeruddin, A. Kay, I. Rodicio, R. Humphry-Baker, E. Muller, P. Liska, N. Vlachopoulos, M. Grätzel, *J. Am. Chem. Soc.* **115**, 6382 (1993)
3. E. Ghadiri, N. Taghavinia, S.M. Zakeeruddin, M. Grätzel, J.-E. Moser, *Nano Lett.* **10**, 1632 (2010)
4. A. Yella, H.W. Lee, H.N. Tsao, C. Yi, A.K. Chandiran, Md.K. Nazeeruddin, E.W.G. Diau, C.Y. Yeh, S.M. Zakeeruddin, M. Grätzel, *Science* **334**, 629 (2011)
5. H.J. Koo, K. Kim, N.G. Park, S. Hwang, C. Park, C. Kim, *Appl. Phys. Lett.* **92**, 142103 (2008)
6. S. Ito, N.L.C. Ha, G. Rothenberger, P. Liska, P. Comte, S.M. Zakeeruddin, P. Péchy, M.K. Nazeeruddin, M. Grätzel, *Chem. Commun.* **38**, 4004 (2006)
7. S.J. Roh, S. Rajaram, S.K. Min, R.S. Mane, W.J. Lee, C.D. Lokhande, S.H. Han, *Appl. Phys. Lett.* **89**, 253512 (2006)
8. P.T. Hsiao, Y.L. Tung, H. Teng, *J. Phys. Chem. C* **114**, 6762 (2010)
9. Y. Alivova, Z.Y. Fan, *Appl. Phys. Lett.* **95**, 063504 (2009)
10. C.Y. Huang, Y.C. Hsua, J.G. Chena, V. Suryanarayanan, K.M. Lee, K.C. Ho, *Sol. Energy Mater. Sol. Cells* **90**, 2391 (2006)
11. B. Liu, E.S. Aydil, *J. Am. Chem. Soc.* **131**, 3985 (2008)
12. O.K. Varghese, M. Paulose, C.A. Grimes, *Nat. Nanotechnol.* **4**, 592 (2009)
13. J.R. Jennings, A. Ghicov, L.M. Peter, P. Schmuki, A.B. Walker, *J. Am. Chem. Soc.* **130**, 13364 (2008)
14. M.K. Nazeeruddin, F.D. Angelis, S. Fantacci, A. Selloni, G. Viscardi, P. Liska, S. Ito, B. Takeru, M. Grätzel, *J. Am. Chem. Soc.* **127**, 16835 (2005)
15. X. Feng, K. Shankar, O.K. Varghese, M. Paulose, T.J. Latempa, C.A. Grimes, *Nano Lett.* **8**, 3781 (2008)
16. B. Liu, J.E. Boercker, E.S. Aydil, *Nanotechnology* **19**, 505604 (2008)
17. H.E. Wang, Z. Chen, Y.H. Leung, C. Luan, C. Liu, Y. Tang, C. Yan, W. Zhang, J.A. Zapien, I. Bello, S.T. Lee, *Appl. Phys. Lett.* **96**, 263104 (2010)
18. H. Wang, Y. Bai, H. Zhang, Z. Zhang, J. Li, L. Guo, *J. Phys. Chem. C* **114**, 16451 (2010)
19. J.H. Bang, P.V. Kamat, *Adv. Funct. Mater.* **20**, 1 (2010)
20. A. Kumar, A.R. Madaria, C. Zhou, *J. Phys. Chem. C* **114**, 7787 (2010)
21. S. Meng, E. Kaxiras, *Nano Lett.* **10**, 1238 (2010)
22. X. Gu, Y.L. Zhao, Y.H. Qiang, *Adv. Mater. Res.* **159**, 306–307 (2011)
23. T.W. Hamann, R.A. Jensen, A.B.F. Martinson, H.V. Ryswyk, J.T. Hupp, *Energy Environ. Sci.* **1**, 66 (2008)
24. W. Lee, S.H. Kang, J.Y. Kim, G.B. Kolekar, Y.E. Sung, S.H. Han, *Nanotechnology* **20**, 335706 (2009)
25. M. Wang, C. Huang, Y. Cao, Q. Yu, Z. Deng, Y. Liu, Z. Huang, J. Huang, Q.G. Huang, W. Guo, J. Liang, *J. Phys. D Appl. Phys.* **42**, 155104 (2009)
26. D. Zhao, T. Peng, L. Lu, P. Cai, P. Jiang, Z. Bian, *J. Phys. Chem. C* **112**, 8486 (2008)
27. M. Murayama, T. Mori, *Thin Solid Films* **509**, 123 (2006)
28. A. Yella, H.W. Lee, H.N. Tsao, C. Yi, A.K. Chandiran, Md.K. Nazeeruddin, E.W.G. Diau, C.Y. Yeh, S.M. Zakeeruddin, M. Grätzel, *Science* **334**, 629 (2011)
29. A. Zaban, M. Greenshtein, J. Bisquert, *Chem. Phys. Chem.* **4**, 859 (2003)